# Tropical Atlantic variability modes (1979–2002). Part I: Time-evolving SST modes related to West African rainfall

Article

Published Version

## www.reading.ac.uk/centaur

**CentAUR**

# Tropical Atlantic Variability Modes (1979–2002). Part I: Time-Evolving SST Modes Related to West African Rainfall

Irene Polo, Belén Rodríguez-Fonseca, Teresa Losada, and Javier García-Serrano

*Departamento de Geofísica y Meteorología, UCM, Madrid, Spain*

## ABSTRACT

This work presents a description of the 1979–2002 tropical Atlantic (TA) SST variability modes coupled to the anomalous West African (WA) rainfall during the monsoon season. The time-evolving SST patterns, with an impact on WA rainfall variability, are analyzed using a new methodology based on maximum covariance analysis. The enhanced Climate Prediction Center (CPC) Merged Analysis of Precipitation (CMAP) dataset, which includes measures over the ocean, gives a complete picture of the interannual WA rainfall patterns for the Sahel dry period. The leading TA SST pattern, related to the Atlantic El Niño, is coupled to anomalous precipitation over the coast of the Gulf of Guinea, which corresponds to the second WA rainfall principal component. The thermodynamics and dynamics involved in the generation, development, and damping of this mode are studied and compared with previous works. The SST mode starts at the Angola/Benguela region and is caused by alongshore wind anomalies. It then propagates westward via Rossby waves and damps because of latent heat flux anomalies and Kelvin wave eastward propagation from an off-equatorial forcing. The second SST mode includes the Mediterranean and the Atlantic Ocean, showing how the Mediterranean SST anomalies are those that are directly associated with the Sahelian rainfall. The global signature of the TA SST patterns is analyzed, adding new insights about the Pacific–Atlantic link in relation to WA rainfall during this period. Also, this global picture suggests that the Mediterranean SST anomalies are a fingerprint of large-scale forcing.

This work updates the results given by other authors, whose studies are based on different datasets dating back to the 1950s, including both the wet and the dry Sahel periods.

## 1. Introduction

The study of the tropical Atlantic (TA) variability (TAV) is an important challenge for the scientific community because its impacts affect a large rural population, which depends on rain-fed agriculture. TAV implies SST patterns, which are linked to extreme climate conditions over the Atlantic basin, and in particular over West Africa (WA).

At interdecadal time scales, the second part of the twentieth century has known a very unusual evolution of Sahelian rainfall with a 20-yr wet period followed by another 20-yr dry period. Such a long-term downward trend in Sahelian summer rainfall is a unique feature in recent tropical fluctuations, and it has been associated with SST trends in the Atlantic and Indian Oceans (Fol-land et al. 1986; Shinoda and Kawamura 1994; Bader and Latif 2003; Giannini et al. 2003; Lu and Delworth 2005). Indeed, this observed drought tendency following the 1960s has been well reproduced with models only forced by observed SST (Giannini et al. 2003; Paeth and Hense 2004; Lu and Delworth 2005; Tippett 2006; Tippett and Giannini 2006). In addition, Zhang and Delworth (2006) have pointed out that the Atlantic multidecadal oscillation, which was in its negative phase in the 1980s–90s, can cause the observed multidecadal variations of Sahel summer rainfall, suggesting that the important role of the multidecadal variability in the interpretation of the recent climate change cannot be ignored.

In spite of this recent understanding about WA rainfall at decadal time scales as well as improvements in seasonal prediction, the general circulation models (GCMs) fail to reproduce WA rainfall interannual variability (Moron et al. 2003; Tippett 2006; Tippett and Giannini 2006). Some authors have suggested that the model error observed in the Sahel rainfall could be

related to the error in the representation of ocean–atmosphere interaction (Tippett 2006). Faced with this, the SST modulation of the interannual variability of WA rainfall during the Sahel dry period deserves more investigation.

At interannual scales, WA rainfall variability is modulated by both oceanic (between 0° and 10°N) and continental (between 10° and 20°N) convergence, by variations in the ITCZ position and land–atmosphere interactions, respectively. Historically, two main WA rainfall types have been identified: dipole years, in which anomalies of opposite signs appear north and south of 10°N, and nondipole years, with anomalies of the same sign in the whole region (Motha et al. 1980; Janicot 1992; Fontaine and Janicot 1996; Ward 1998). This classification, based on the available in situ precipitation data from land stations over WA, has been useful in order to discriminate some associated processes and SST influences (Fontaine and Janicot 1996; Janicot et al. 1998; Ward 1998). However, it accounts for a large variability occurrence in the different wet and dry decadal periods over the Sahel (Janicot et al. 1996; Ward 1998; Janicot et al. 2001). Some of these studies have suggested that the occurrence of dipole years, which are most closely associated with TA SST, is dominant during the wetter epoch, whereas nondipole years are particularly numerous in the dry Sahel period (Ward 1998; Janicot et al. 2001), when the ENSO is more active in relation to WA rainfall (Janicot et al. 1998; Janicot et al. 2001). Paeth and Stuck (2004) have suggested that warm TA SSTs could enhance the rainfall dipole, which is the prevailing precipitation pattern in the Climatic Research Unit (CRU) observational dataset as well as in the global and regional climate models outputs. However, some discriminant analyses have shown perfect uncoupled rainfall variability modes between the Sahel and the coast of the Gulf of Guinea (GG), associated with different global SST anomalies (Ward 1998; Giannini et al. 2003). This work will present rainfall patterns calculated from the enhanced satellite-based Climate Prediction Center (CPC) Merged Analysis of Precipitation (CMAP) dataset, which includes measures over the ocean, a feature that needs to be discussed with respect to other WA rainfall observational studies.

Regarding rainfall variability on the coast of the GG, it seems to have a very tight ocean–atmosphere coupling at interannual and decadal time scales (Wagner and da Silva 1994; Fontaine and Janicot 1996; Ward 1998; Vizy and Cook 2001; Giannini et al. 2003), linked with the well-known Atlantic El Niño mode (Zebiak 1993; Carton et al. 1996). Vizy and Cook (2001) have shown that such SST events enhance evaporation, and

that the southerly flow across the coast of the GG carries more moisture inland, leading to increased precipitation south from the usual latitude of the ITCZ. The Atlantic El Niño mode is characterized by a relaxation in the equatorial trade winds, which induces a redistribution of warm water in the equatorial belt and a weakening in the equatorial thermocline slope and also in the heat content zonal gradient (Carton et al. 1996; Vauclair et al. 2004). In cold years (dry years in the GG region), the northward ITCZ movements can begin as early as February. Conversely, the warm years (wet years over the GG) are characterized by a reduction of the southerly flow between April and June, followed by a rapid increase later in July (Fontaine et al. 2003). Although the Atlantic El Niño has been investigated from the 1980s, the related air–sea interaction mechanisms are still a current topic (Keenlyside and Latif 2007), mainly because of the lack of reliable ocean data in the TA. This work makes a dedicated effort to address the main question about the development and damping of this SST mode coupled to GG rainfall.

The relation between the Sahelian rainfall and the so-called Atlantic SST meridional mode (Chang et al. 1997) was pointed out to be more important before 1970, during the wet Sahel period (Janicot et al. 1996; Janicot et al. 2001) and at interdecadal time scales (Lamb 1978; Hastenrath 1984). However, the role of the subtropical North Atlantic (SNA) SST on WA rainfall is still unclear. Some authors have suggested that SNA SST plays a passive role with regard to WA rainfall (Ward 1998; Mo et al. 2001). Vizy and Cook (2001) suggest that this region can have less influence over the Sahelian rainfall, mainly because the low-level flow between the SNA and WA is a northeasterly flow, which tends to isolate the continent from SNA, and because horizontal advection is not very effective in the tropics. However, from their GCM simulations, a response to positive SNA and GG SST anomalies results in a westerly low-level flow perturbation that largely impacts WA precipitation (Vizy and Cook 2001).

The possible Sahelian impact from other regions, such as the Mediterranean Sea, has also been supported (Rowell 2001). From AGCM simulations, Rowell (2003) has found positive Mediterranean Sea SST anomalies related to anomalous positive Sahel rainfall through evaporation and southward moisture advection that enhances low-level convergence over the Sahel. Jung et al. (2006) have simulated significant increased Sahelian rainfall for the warm Mediterranean event of 2003, derived from enhanced evaporation in the Mediterranean Sea. Nevertheless, there is still an open question about whether the Mediterranean basin plays an

effective role or it is only a fingerprint of larger-scale forcing.

Regarding the global signature of the TAV, some studies have evidenced an association between ENSO events and the Atlantic El Niño mode (Latif and Grötzner 2000; Wang 2006), and both phenomena are related to WA rainfall patterns (Rowell 2001; Janicot et al. 1998; Janicot et al. 2001). ENSO seems to act by modifying the east–west divergent circulation, which modulates the vertical movements over WA, while the Pacific–Atlantic zonal atmospheric gradient, coupled to the opposite SST anomalies over both oceanic basins, can enhance the WA rainfall response (Janicot et al. 1998). However, the setup of a Pacific–Atlantic zonal atmospheric oscillation in the dry Sahel period could be the result of recent changes in the anomalous SST and WA rainfall trends after 1970. The Pacific–Atlantic relationship has dramatically changed in this recent period (Keenlyside and Latif 2007), and therefore the study of such a relationship is important for understanding the interannual influences over WA.

The aim of this work is to clearly identify and describe the SST modes of variability over the WA adjacent oceans that are coupled to summer WA rainfall during the 1979–2002 period, and their seasonal time evolution (origin, development, and damping). To accomplish this objective, we have developed an extended methodology of the classical maximum covariance analysis (MCA) and applied it to the WA monthly anomalous summer [June–September (JJAS)] precipitation and the monthly TA and Mediterranean SST anomalies from February–May (FMAM) to September–December (SOND). Because the methodology highlights the seasonal dependence of the time-evolving SST, it will give new and valuable insight on the understanding of these interannual variability modes.

The SST patterns found in this paper are being used as boundary conditions in some of the sensitivity experiments that the African Monsoon Multidisciplinary Analysis (AMMA)-European Union (EU) project has planned to perform with different AGCMs, with the aim of understanding the response of the WA rainfall to the SST in the adjacent oceans and its potential predictability. The same extended maximum covariance analysis (EMCA) methodology has been applied in García-Serrano et al. (2008), focusing on the relation between the summer TA SST patterns and summer–winter Atlantic precipitation variability, addressing the TAV–extratropical connection through tropical convection.

In the next section 2, the data and the methodology used in this work are described. Section 3 describes the principal components of the WA rainfall and the main SST–WA rainfall covariability modes. The air–sea interactions related to the leading SST pattern, as well as the global SST signature of every mode, are analyzed. Finally the main conclusions are discussed in section 4.

## 2. Data and methodology

The 1979–2002 monthly CMAP (Xie and Arkin 1997) and extended reconstructed sea surface temperature (ERSST) dataset (Smith and Reynolds 2003) for the SST variable have been used to study the main coupled modes between summer WA precipitation and TA SST. Regarding data accuracy, 1979–2002 is very reliable period because satellite data are included in the precipitation datasets. Also, the use of these data provides information on the precipitation over the ocean, something important if we want to follow the patterns over the basin. As a first step of the analysis, JJAS monthly standardized precipitation empirical orthogonal functions (EOFs) are computed to quantify the principal modes of WA precipitation during the whole monsoon season. Then, the anomalous SST patterns coupled to the summer WA rainfall variability is described and analyzed. Eight different 4-month sequences, centered in JJAS, and lagging 1 month forward and backward, are computed to find the state of the ocean in relation to the WA rainfall variability. Time series are linearly detrended and anomalies are calculated with respect to the considered period.

To follow and give an interpretation of the air–sea processes related to the leading SST coupled mode, several oceanographic and atmospheric key variables have been analyzed. The oceanic variables are the wind stress [from the Pilot Research Moored Array in the Tropical Atlantic (PIRATA) dataset; see Servain et al. (1998)], the 20°C isotherm depth as tropical thermocline depth proxy [from the Tropical Atlantic Ocean Subsurface Temperature Atlas (TAOSTA) dataset; see Vauclair and du Penhoat (2001)], and the sea level anomalies [SLAs; from the altimetry measures of the Ocean Topography Experiment (TOPEX)/Poseidon in the period of 1993–2001, which is provided by Centre National d'Études Spatiales (CNES) Archiving, Validation, and Interpretation of Satellite Oceanographic data (AVISO)]. The atmospheric variables are the interpolated outgoing longwave radiation [OLR; provided by the National Oceanic and Atmospheric Administration (NOAA)/Office of Oceanic and Atmospheric Research (OAR)/Earth System Research Laboratory (ERSL) Physical Sciences Division (PSD); see Liebmann and Smith 1996], surface heat fluxes, surface winds, and sea level pressure (SLP). The latter surface variables come

from the 40-yr European Centre for Medium-Range Weather Forecasts (ECMWF) Re-Analysis (ERA-40) dataset (Uppala et al. 2005), which includes satellite data from 1973.

The methodology of EMCA (Fig. 1) is developed and implemented in this study. This methodology is an extension of the maximum covariance analysis (Bretherton et al. 1992, Frankignoul and Kestenare 2005; Polo et al. 2005), but considers all of the lagged SST time series in the same array (see Fig. 1, matrix Y). Using EMCA we can isolate, in the same mode, the whole sequence of significant covariant SST patterns in relation to the JJAS precipitation, and accomplish the whole picture of the SST pattern evolution in relation to the precipitation with a realistic persistence feature from boreal late winter to summer. Because the TA SST signals can develop rapidly from early spring to late summer, in our method, a priori, we do not discriminate between the season of the maximum SST covariability and the summer rainfall (in contrast with the classic MCA).

In addition, EMCA gives the opportunity for increasing the number of time series in the analysis, having as many time series per point as time lags used in the analysis, and in this way assesses the statistical significance of the results. As in the classical MCA, each mode comprises different spatial structures (singular vectors) and time series (expansion coefficients) for every involved field in the analysis. The results are shown in terms of homogeneous and heterogeneous regression maps, for the SST sequence and the summer precipitation field, respectively. For each mode, the SST homogeneous map (HM) shows the amplitude of the projection (for each grid point and each lag) of the total SST expansion coefficient onto the TA SST anomalies, giving a measure of the SST anomaly per standard deviation. The precipitation heterogeneous maps (HT) show the amplitude of the projection of the total SST expansion coefficient onto summer WA rainfall anomalies, giving a measure of the precipitation anomalies associated with one standard deviation of the anomalous SST. Only those areas that are 98% statistically significant (evaluated with a $t$ test) are mapped. A measure of the fraction of explained covariability [square covariance fraction (SCF)], and the correlation coefficient (RUV) between the independent and dependent expansion coefficients complete the information for each mode. To quantify the statistical significance of the EMCA, additional statistical information is given. To test if the SST–precipitation link found is not random, we have checked the results using a Monte Carlo test. In this way, the combined action of shuffling and applying the EMCA is performed 100 times. The prob-

ability density function of the SCF parameter that arises from these 100 realizations is compared to the nonshuffled EMCA SCF scores, giving a significance level (SL) for the connection found.

## 3. Results

### a. Principal component analysis

In this section, interannual WA rainfall modes (over the region 5°S–32°N, 21.25°W–33.75°E) are computed for the dry Sahel period using the CMAP dataset, with the aim of updating the results given by previous authors. The first two EOFs of WA monthly standardized anomalous precipitation during the rainy season (JJAS), which account for around 20% of the total variance, are shown in Fig. 2. The following third mode has not been considered because its sampling error is larger than the spacing between second and third eigenvectors, which means that the third PC is part of a degenerate multiple (North et al. 1982). The significant precipitation pattern of the leading principal component (PC) shows the anomalous Sahelian rainfall (*Sahelian mode*, see Fig. 2a) as the first mode, with more no-rain than wet periods during the whole sequence. This pattern accounts for 10% of the total variance and its study is of great importance because it explains part of the WA monsoon variability, which is a hot topic for the agriculture and health in developing countries (Sultan et al. 2005). The regression map of the second PC represents the rainfall pattern of the coast of the GG (*Guinean mode*, see Fig. 2b). The pattern exhibits interannual and interdecadal variability, with more dry events over the coast of the GG in the 1990s than in the 1980s.

While other works present the Guinean mode as the leading WA rainfall mode (Giannini et al. 2003), from our results during 1979–2002, most of the rainfall interannual variability is concentrated over the Sahel region, with the Guinean mode being the second EOF. A prior normalization of the rainfall anomalies has confirmed the reversion of the order of the first two modes (not shown). Without the standardization of the rainfall anomalies (as done in Giannini et al. 2003), the rainfall anomalies of the coast of the GG have higher amplitudes and appear as the leading mode.

In addition, although several authors have pointed out that a significant part of the interannual variability of WA anomalous rainfall is due to the opposite evolution between central Sahelian and Guinean rainfall indexes as a dipole pattern (Janicot 1992; Fontaine et al. 1995; Fontaine and Janicot 1996; Ward 1998; Douville et al. 2007), our results separate the Sahelian and the Guinean rainfall in two different modes. Further-

# EMCA
## Extended Maximum Covariance Analysis

X=precip
JJAS

$X=X(ns_{precip},nt) \rightarrow$ precip JJAS
$Y1=Y1(ns_{sst},nt) \rightarrow$ SST FMAM
$Y2=Y2(ns_{sst},nt) \rightarrow$ SST MAMJ
$Y3=Y3(ns_{sst},nt) \rightarrow$ SST AMJJ
$Y4=Y4(ns_{sst},nt) \rightarrow$ SST MJJA
$Y5=Y5(ns_{sst},nt) \rightarrow$ SST JJAS
$Y6=Y6(ns_{sst},nt) \rightarrow$ SST JASO
$Y7=Y7(ns_{sst},nt) \rightarrow$ SST ASON
$Y8=Y8(ns_{sst},nt) \rightarrow$ SST SOND

Y1=SST
FMAM

Y2=SST
MAMJ

Covariance matrix  C/
$$C=X(ns_{precip},t)*Y^T(t,8*ns_{sst})$$

$\Downarrow$
$\Downarrow$

Y3=SST
AMJJ

Y=

$$[R,U]=eig(C*C^T)$$
**R**: spatial precip patterns related to SST

Y4=SST
MJJA

**U**: precip expansion coefficients

$\Downarrow$
$\Downarrow$

Y5=SST
JJAS

$$[Q,V]=eig(C^T*C)$$
**Q**: spatial SST patterns related to precip/
$Q=[Q_{1(FMAM)}\ Q_{2(MAMJ)}\ Q_{3(AMJJ)}\ Q_{4(MJJA)}$
$Q_{5(JJAS)}\ Q_{6(JASO)}\ Q_{7(ASON)}\ Q_{8(SOND)}]$

Y6=SST
JASO

**V**: SST expansion coefficients /

Y7=SST
ASON

$V=V_{1(FMAM)}+V_{2(MAMJ)}+V_{3(AMJJ)}$
$+V_{4(MJJA)}+V_{5(JJAS)}+V_{6(JASO)}+V_{7(ASON)}$
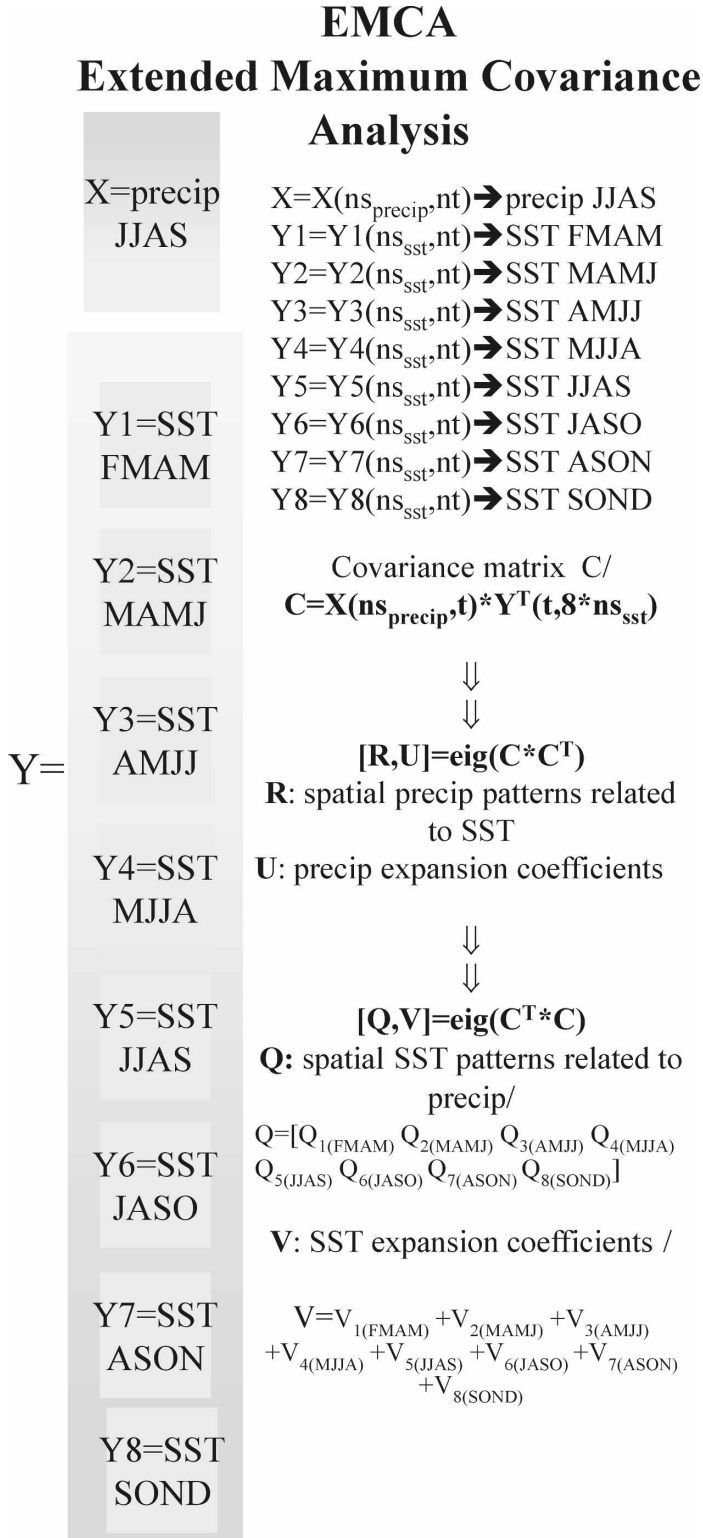$+V_{8(SOND)}$

Y8=SST
SOND

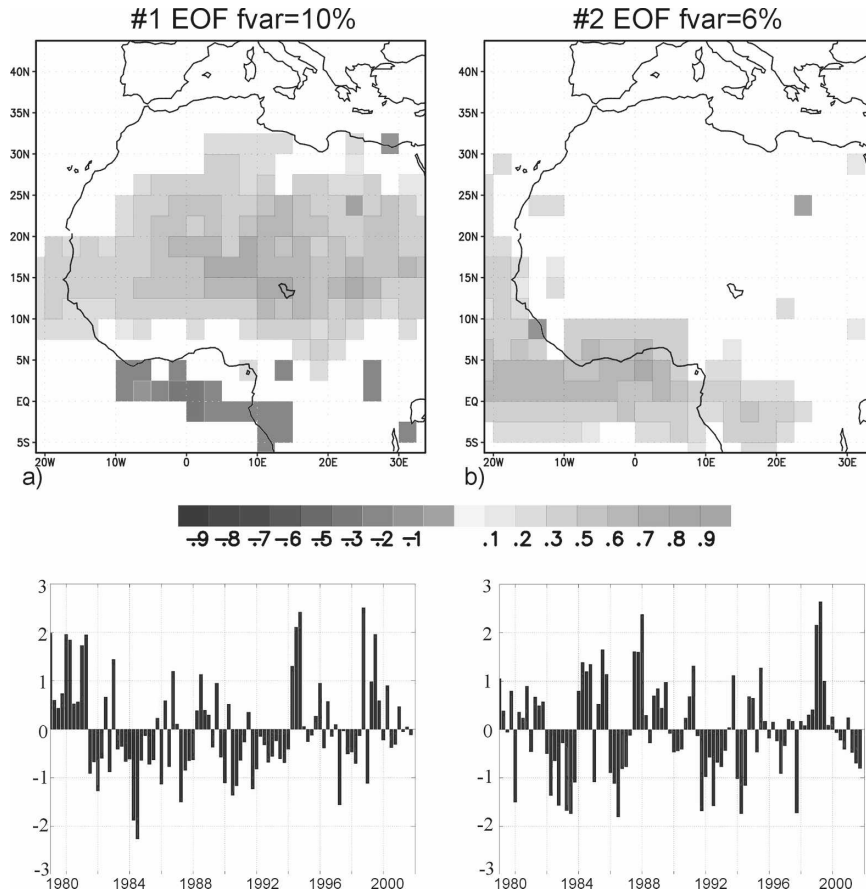FIG. 1. Scheme of the EMCA used in this study.

FIG. 2. First two CMAP JJAS precipitation EOFs over WA. Only 98% statistically significant areas (SSA), evaluated with a *t* test, have been shaded. Times series of the associated PCs are in bars.

more, the dipole classification operates under the assumption that both the Sahel and the coast of the GG have the same variability patterns; however, it is clear that they have different variability, especially in the last dry period (Ward 1998). Because the processes associated with both are operating and competing (Ward 1998) for some analysis, the dipole and nondipole subdivisions appear useless. The absence of the dipole pattern in our analysis could be caused by the dataset used; CMAP rainfall comes from satellite data with land–sea continuity and a smaller time span (1979–2002), which is contained in the dry Sahel period. To check this hypothesis, we have analyzed the same patterns considering the CRU dataset for a longer period (1949–96) and for part of the dry period (1975–96). For the same data treatment and for both periods, we have obtained the same uncoupled Sahelian and Guinean modes (not shown). Likewise, standardization produces a reversal of the modes in the sense of percentage of variability. A kind of dipole pattern is found for the second period without standardizing the WA rainfall anomalies, al-

though it has the maximum loadings over the coast of GG region. Therefore, this data treatment dependence reveals that the dipole is not robust enough to be considered as a canonical pattern.

### b. SST–precipitation coupled modes

To determine the TA SST patterns related to summer WA precipitation anomalies, we apply EMCA between the TA SST from FMAM to SOND and JJAS WA rainfall. For the leading EMCA mode, which accounts for 31% of the SCF, the SST significant homogeneous regression maps shows positive SST anomalies over the Atlantic equatorial tongue region from the previous spring (AMJJ), related to an increase of summer precipitation along the coast of the GG (Fig. 3, upper panel). The precipitation expansion coefficient of this mode has a strong relation to the Guinean mode in Fig. 2b (0.89 correlation coefficient), and the SST expansion coefficient is very well correlated (0.84 correlation coefficient) with the equatorial Atlantic SST index (ATL3; Zebiak 1993), which describes the Atlan-
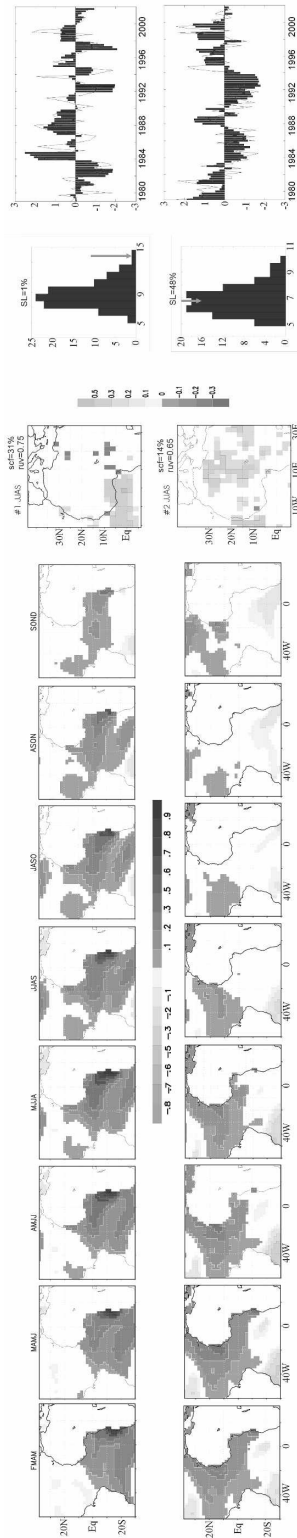
FIG. 3. First two covariability modes obtained from the EMCA between summer WA precipitation and the anomalous SST (°C) 4-month sequences from FMAM to SOND. SSA as in Fig. 2. The probability density function of the SCF from 100 times Monte Carlo tests (histogram) is compared with the original EMCA SCF score (arrow) to show its significance level. The expansion coefficients (SST in bars, precipitation in continuous line) are shown for each mode.

tic El Niño mode. It is important to mention that the Guinean rainfall pattern appears now as the leading mode of covariability with TA SST, implying that an important part of the rainfall variability of the coast of the GG can be explained by TA SST anomalies. Conversely, Sahelian rainfall has been related to more global SST patterns, such as the Pacific (Giannini et al. 2003; Janicot et al. 1998) and Indian or northern basin ocean (Giannini et al. 2003; Ward 1998), and to land surface processes (Douville 2002; Philippon and Fontaine 2002).

The second EMCA mode (Fig. 3, lower panel) represents 14% of the total SCF and describes a spatial pattern with positive summer rainfall anomalies over the Sahel and positive SST anomalies over the SNA and Mediterranean Sea, persisting for some months in advance. The precipitation expansion coefficient has a strong relation to the Sahelian mode in Fig. 2a (0.87 correlation coefficient). Nevertheless, this is not a robust mode because the SL obtained from the Monte Carlo test indicates that the results can be reproduced in half of the shuffled cases. For this reason, this mode will be discussed and recalculated in the next sections.

In the following section, these two covariability modes are intensely analyzed: on the one hand the leading mode, which corresponds to the Guinean rainfall and the Atlantic El Niño, is discussed in terms of air–sea interactions; and on the other hand the second covariability mode will be analyzed and discussed in order to better understand the role of the SNA and Mediterranean Sea SST on the Sahelian rainfall. The global picture of these SST patterns will also be discussed.

### 1) EQUATORIAL ATLANTIC SST–GUINEAN RAINFALL MODE: AIR–SEA INTERACTIONS

Figure 3 (upper panel, from FMAM to SOND) shows the sequence of SST homogeneous regression maps, related to the Atlantic El Niño or equatorial mode (EM), linked to the Guinean anomalous precipitation. Here, it can be seen that the EM develops from FMAM to JJAS, starting with a maximum of anomalous SST over the Angola/Benguela upwelling region, with a second relative maximum around 20°S. Afterward, the mode shows a strengthening and/or northward (westward) propagation of the coastal (equatorial) anomalies and a weakening of the anomalies in 20°S. Then, the whole mode starts to weaken, disappearing in SOND. The Bjerknes mechanism components in the EM have been analyzed by other authors (Keenlyside and Latif 2007), but there are still some gaps regarding the development and damping of the mode. Therefore, we will analyze the thermodynamics
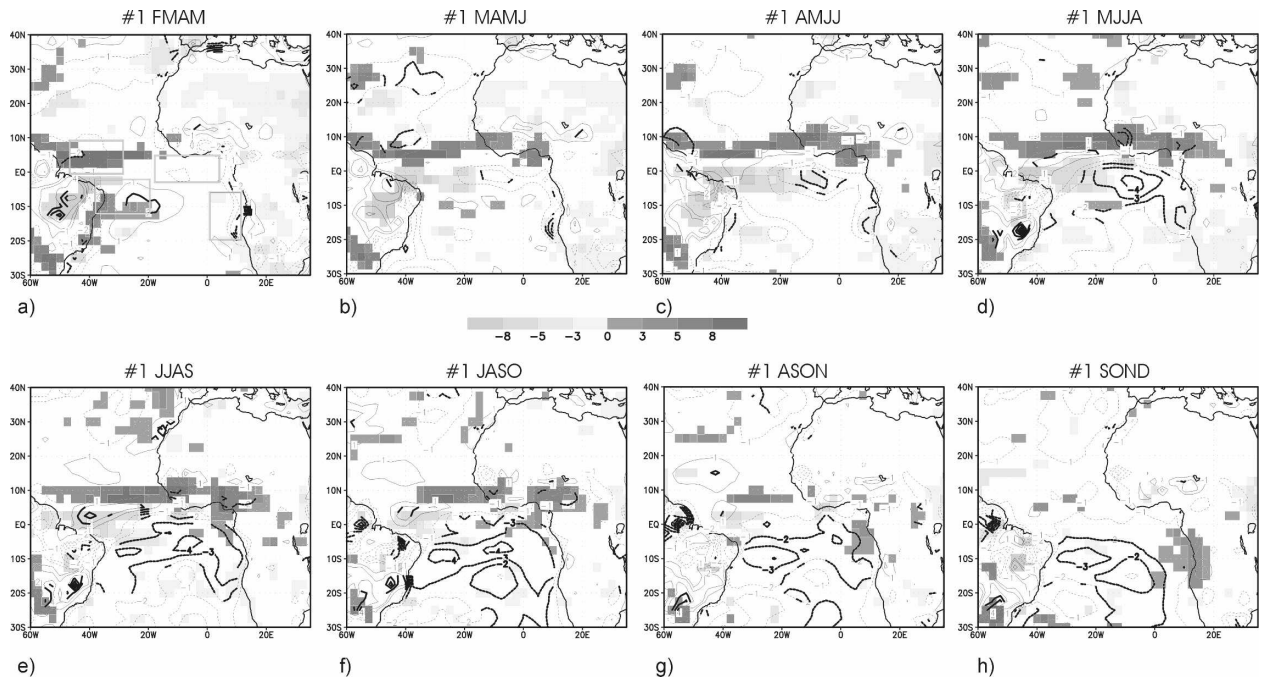
FIG. 4. Regression of the total SST expansion coefficient associated with the leading EMCA mode onto the radiative flux anomalies [shortwave − longwave radiation (W m$^{-2}$), positive downward], and the latent heat flux anomalies [contour interval (CI) = 1 W m$^{-2}$, positive downward] for the 4-month sequences from (a) FMAM to (h) SOND. The boxes in (a) are regions considered in the heat balance. SSA as in Fig. 2.

and dynamics involved in the mode's evolution by regressing the SST expansion coefficient onto different thermodynamic and oceanographic variables.

The role of the TA heat fluxes in relation to the EM is investigated in Fig. 4, which shows the balance between the radiative fluxes (shortwave radiation minus longwave) and the turbulent fluxes (latent heat fluxes). Regarding the EM evolution from FMAM to JJAS, heat fluxes are not responsible for the SST anomalies located in the Benguela upwelling region (10°–20°S, 0°–10°E), because the SST warming is concomitant with more evaporation over this region. On the contrary, the west-equatorial North Atlantic warming (0°–10°N, 50°–30°W) can be attributed to an increase of solar radiation (associated with less clouds) and a decrease of evaporation. The damping of the SST anomalies at the southern lobe (0°–10°S; 40°–20°W) starts in MAMJ because of an increase of the latent heat flux to the atmosphere and a decrease of the solar radiation. From JJAS to SOND, negative latent heat flux anomalies could be responsible for the damping at the south of the tongue, while radiative fluxes reduce the SST anomalies at the east, in agreement with Trzaska et al. (2007). From the thermodynamics analysis of the EM, we conclude that, although both negative radiative and latent heat fluxes anomalies could be important in damping

the SST in the EM, heat fluxes cannot explain the generation and persistence of the SST anomalies at the southeastern region.

To find an explanation for the SST anomaly generation at the southeastern part of the tongue from the previous winter, regression of the SST expansion coefficient onto the surface winds and the SLP is displayed in Fig. 5. Noticeable is an enhancement of the clockwise circulation, together with a weakening of the subtropical Santa Helena high pressure system from the previous November–February (NDJF) winter sequence. Such a feature could be responsible for the anomalous southeastward surface winds, and hence the SST warming. However, both wind anomalies over the eastern South Atlantic and positive SST anomalies over the Benguela region (not shown) are significant 2 months before negative SLP anomalies from SOND. At that moment, positive SLP anomalies cover the Amazon basin and the equatorial band (Figs. 5a,b) suggests that subsequent weakening of the Santa Helena high could be forced by inversion of the local Hadley cell via an atmospheric bridge. Such a type of mechanism has been proposed in the Northern Hemisphere for explaining the anomalous indirect Atlantic Hadley circulation during the mature and decay phases of El Niño (Wang 2002a,b). However, this result is not totally in agree-
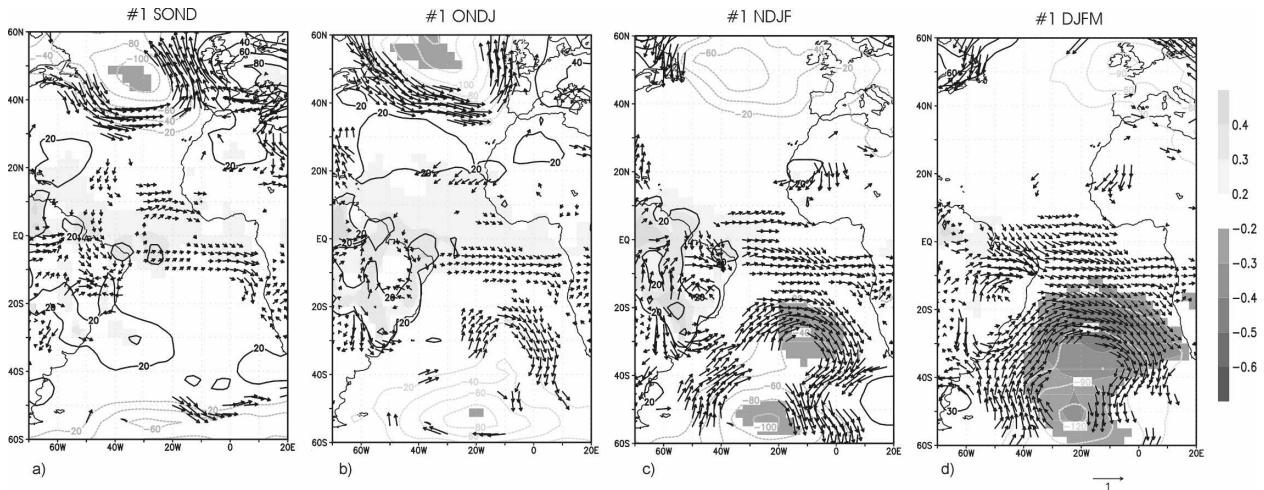
FIG. 5. Regression of the total SST expansion coefficient associated with the leading EMCA mode onto the surface wind anomalies [vectors (m s$^{-1}$)] and the SLP (CI = 20 mbar, SSA as in Fig. 2 have been shaded) for the 4-month sequences from previous (a) SOND to (d) DJFM. SSA as in Fig. 2.

ment with other authors' findings. Trzaska et al. (2007) have shown the EM as a consequence of the subtropical South Atlantic (SSA) SST mode (consistent with Venegas et al. 1997), which is associated with the south Atlantic subtropical high SLP anomalies, and no mention is made of the equatorial contribution.

Despite most of the works being associated with the origin and development of the EM with subtropical atmospheric dynamics, some authors have suggested that Ekman pumping and the wind stirring may also play a role in the SST evolution over the TA (Sterl and Hazeleger 2003; Barreiro et al. 2004). In view of this, the oceanic component is analyzed in Fig. 6, which shows the regression of the leading EMCA mode SST expansion coefficient onto the wind stress and the Ekman pumping. Figure 6a (and Figs. 5a,b) shows how, from the previous winter months, anomalous southward wind stress locally changes the upwelling over the Benguela front, and thus the SST and the thermocline depth over the region (not shown). In particular, in December–March (DJFM), this positive SST anomaly over the southern Atlantic produces a meridional and zonal basin gradient, which increases the northwesterly wind stress over the south Atlantic (Fig. 6b). From DJFM to April–July (AMJJ; see Figs. 6b,e), southeastward anomalous wind stress changes the thermocline slope, rising at the west and sinking at the east in the equator (not shown). In March–June (MAMJ; see Fig. 6d) in the southwest Atlantic, the wind stress curl starts to be anomalously cyclonic, creating upward Ekman pumping and cooling the mixed layer at the west-central basin as the latent heat flux decreases (Fig. 4c). From July to October (JASO), the positive Ekman

pumping anomalies are located over the eastern part of the basin, because the southerly alongshore wind starts to be significant over 10°S, helping to damp the mode.

The SLA pattern associated with the EM consists of an anomalous eastern equatorial Atlantic tongue (as the SST) and a western equatorial Atlantic with an opposite sign SLA, in a seesaw-like thermocline configuration (not shown), in agreement with other authors (Wang 2006; Keenlyside and Latif 2007). Because the EM strongly involves subsurface equatorial dynamics through equatorial wave adjustment (Vauclair and du Penhoat 2001; Vauclair et al. 2004; Handoh and Bigg 2000), and because we are looking for a mechanism that could explain the development of the EM (from winter to summer) on the one hand and the fading of the EM (from summer to autumn) on the other, time–longitude plots of SLA have been done for extreme positive and negative events of the expansion coefficient. We have chosen years 1995 and 1997, positive and negative EM years, respectively (see expansion coefficients in Fig. 3, upper panel), following the SLA from 40°W to 10°E and from February to October.

For 1995 (1997), the time–longitude SLA plots (Fig. 7) at 5°S show how the positive (negative) SLA signal at the southeast Atlantic is propagating clearly westward as a Rossby wave (Chelton and Schlax 1996; Polito and Cornillon 1997). This eastern perturbation travels as far as 30°–20°W and does not propagate farther west (Figs. 7a,b, left), because an anomaly of the opposite sign appears. This SLA could be originated and/or reinforced by the Ekman pumping at this longitude, from the AMJJ season, and it is also propagating westward with the same phase speed, cancelling the
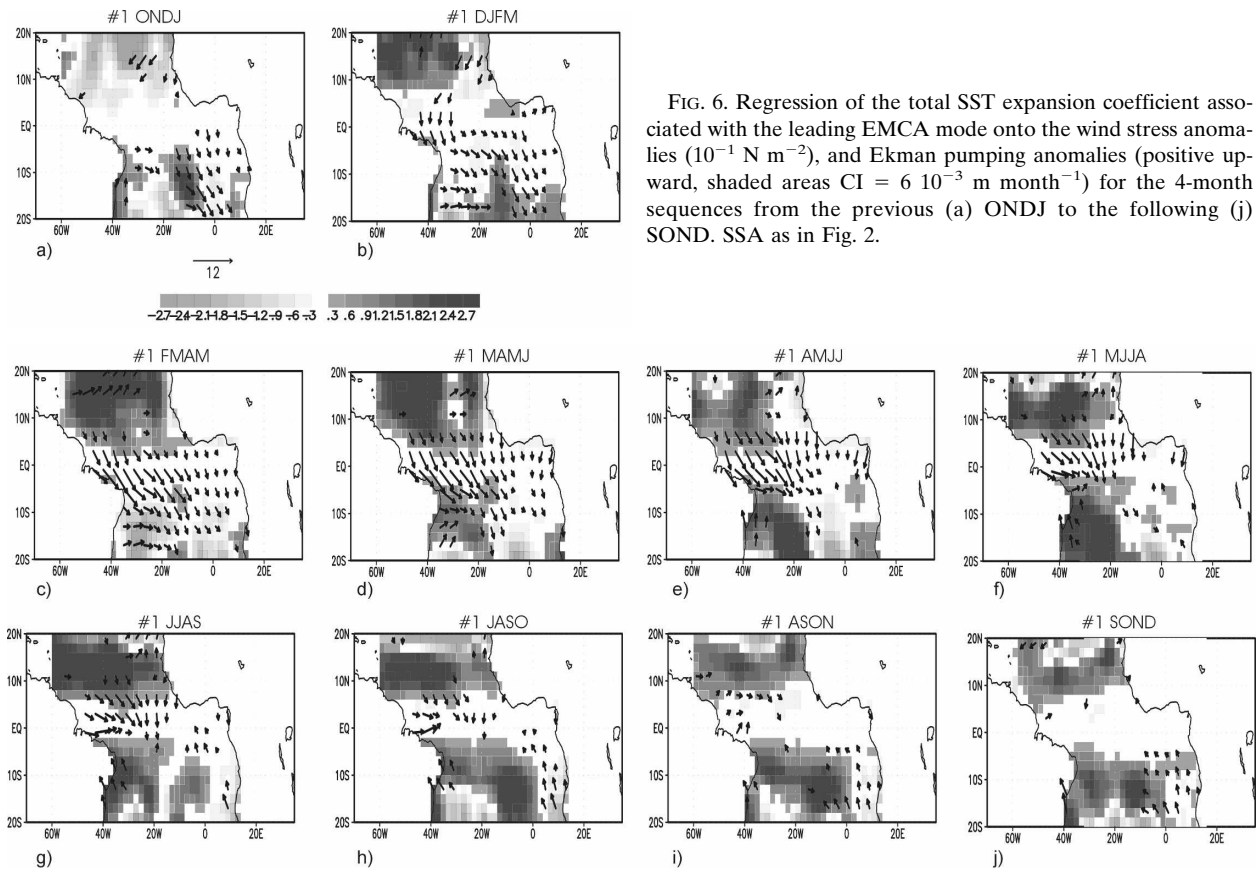
FIG. 6. Regression of the total SST expansion coefficient associated with the leading EMCA mode onto the wind stress anomalies ($10^{-1}$ N m$^{-2}$), and Ekman pumping anomalies (positive upward, shaded areas CI = 6 $10^{-3}$ m month$^{-1}$) for the 4-month sequences from the previous (a) ONDJ to the following (j) SOND. SSA as in Fig. 2.

positive (negative) SLA propagation farther west. Simultaneous with the westward upwelling (downwelling) Rossby wave traveling along 5°S (Figs. 7a,b, left), there is an upwelling (downwelling) Rossby wave traveling westward along 5°N latitude (not shown); the wind stress over 30°–20°W is also favoring (inhibiting) the Ekman pumping at both sides of the equator for 1995 (1997). At the beginning of July, this negative (positive) SLA signal appears in the western equatorial Atlantic and is reflected as an eastward Kelvin wave traveling up to September reaching the eastern equator (Figs. 7c,d, right), and helping to damp the EM. The wind stress anomalies over 30°–20°W, the associated Ekman pumping at both sides of the equator (Fig. 6g), and the possible relation to anomalous SLA signal, triggering a Kelvin wave, support the hypotheses proposed by Polo et al. (2008) that Ekman pumping ITCZ shift-induced anomalies are, in part, a source for equatorial Atlantic Kelvin waves.

Although the hypothesis needs to be checked using a model, we have found that the EM starts at the Angola/Benguela upwelling region. The SLAs radiate and propagate westward as Rossby waves, and damp because of the latent heat flux anomalies at the South

Atlantic and the Kelvin wave eastward propagation from an off-equatorial forcing. The phase speed for the westward and eastward propagation has been computed with the radon transform technique (Hill et al. 2000). The mean phase speed calculated for the westward propagation at 10°, 5°, and 2.5°S is −0.5 m s$^{-1}$, and for the equatorial eastward propagation it is around 3 m s$^{-1}$, corresponding approximately to the first baroclinic mode (Philander 1990; França et al. 2003). Longitudinally, the area around 30°–25°W seems to be a threshold for the first baroclinic Rossby wave. Nevertheless, for both westward Rossby wave and eastward Kelvin wave propagations there is more homogeneity in the middle of the basin (from 20° to 5°W). In addition, other nonlinear processes could interfere in the propagation continuity onshore; however, these tasks are out of the scope of this study and future research lines.

Our results presented above disagree with Latif and Grötzner (2000), Florenchie et al. (2003), and Wang (2006) with regard to the oceanic wave propagation's role in the origin of the equatorial and South Atlantic SST variability. In particular, Florenchie et al. (2003) have suggested that the generation of the Benguela El
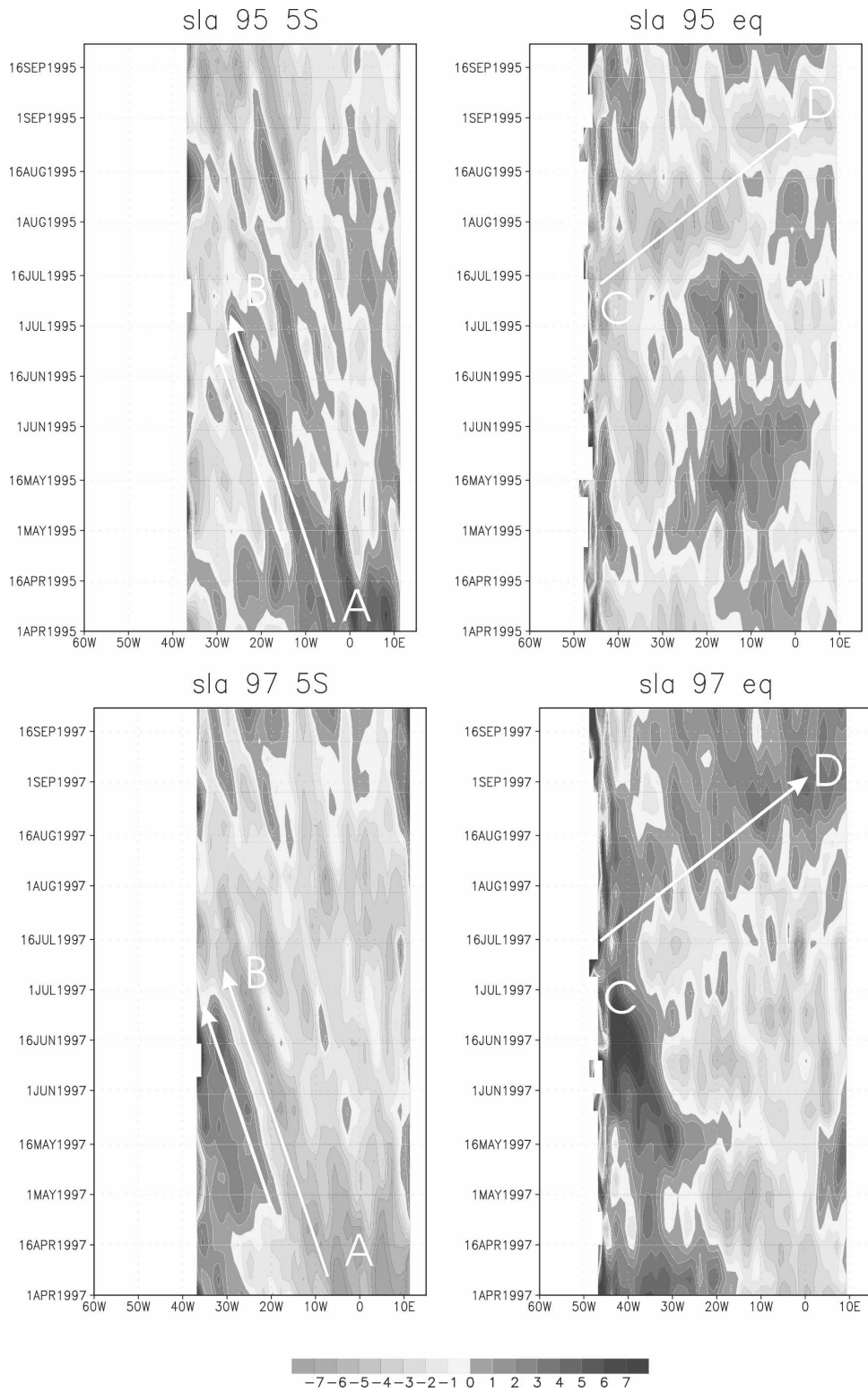
FIG. 7. SLAs (cm) from April to September along (left) 5°S and (right) the equator for (top) 1995 and (bottom) 1997.

Niños could be remotely generated by wind anomalies at the west-central equatorial Atlantic via oceanic Kelvin wave propagation, and Wang (2006) has supported this result. Also, Latif and Grötzner (2000) have showed an eastward SLA propagation from the western equatorial Atlantic in winter that reaches the eastern equatorial Atlantic the next summer when it can be amplified by air–sea interactions and the SST can be modified. Our results show that neither west-equatorial Atlantic SLA in winter nor anomalous winds in the west-central equatorial Atlantic have been found to force Benguela El Niños/EM via Kelvin waves.

Regarding the Pacific–Atlantic connection, Latif and Grötzner (2000) showed how, at quasi-biennal time scales, a winter El Niño event leads an Atlantic El Niño the following summer with no significant simultaneous relationship. Recently, Wang (2006) has discussed the importance of the Pacific–Atlantic SST gradient driving the atmospheric circulation across equatorial South America via the SLP gradient and influencing the tropical climate variability in a feedback way. To assess these relationships between basins, the EM has been regressed onto the global SST and precipitation anomalies (Fig. 8), showing a global rainfall pattern that involves the whole tropical belt. The equatorial Atlantic positive precipitation anomalies from FMAM to AMJJ are related to negative precipitation anomalies over the central Pacific. From JJAS to SOND, the Atlantic El Niño is being damped, with a westward displacement of the global tropical convection anomalies increasing the West Asian precipitation and decreasing the central to eastern Pacific precipitation (La Niña–like pattern). This is more evident when considering the global SST anomalies associated with the EM: SST anomalies decrease from the central to the east Pacific Ocean and increase at the western Pacific (Figs. 8a,d contour lines). To address a possible EM modulation, we have correlated the lagged Niño-3 index with the EMCA SST expansion coefficient (Fig. 8e). The maximum correlation occurs when a warm EM phase in summer leads the Pacific La Niña by 6–8 months during the following winter. This is a very relevant result that points out a different equatorial Pacific–Atlantic connection in the 1979–2002 period: the Atlantic El Niño can lead the Pacific La Niña, and this situation seems to be related to the Guinean rainfall mode instead of Sahelian rainfall. Jury et al. (2002) have found that upper zonal winds in the central Atlantic lead the Niño-3 SST index, particularly in the 1980s and 1990s. They suggest that both the Niño-3 and the Atlantic winds are responding to atmospheric convective forcing in the western Pacific, but that the upper wind reacts more quickly to eastward-shifted convection in the Pacific than the

Niño-3 SST, which depends on the comparatively slow eastward propagation of ocean anomalies. These upper winds could force, through the Walker circulation, the SST in the tropical Atlantic to react more quickly that the Niño-3 SST, explaining in this way the relation found between the Atlantic and the Pacific. Melice and Servain (2003) have also shown the south tropical Atlantic leading the Southern Oscillation index (SOI) from 1984 to 1998 by ~4 months, although they do not know how the south tropical Atlantic could be dynamically linked with the Southern Ocean or even if such a link exists. Nevertheless, the importance of the later result in Fig. 8, regarding the recent trends in the Pacific–Atlantic connection, needs further investigation and will be the focus of future studies.

### 2) Subtropical North Atlantic and Mediterranean Sea SST–Sahelian rainfall mode: A discussion

In JJAS, the second mode in Fig. 3 (lower panel) associates the Sahelian anomalous rainfall with Mediterranean Sea SST anomalies, persisting from FMAM, and SNA SST anomalies, damping from AMJJ. The Mediterranean Sea influence on the WA monsoon regime has already been evidenced (Rowell 2001) and studied with AGCM simulations (Rowell 2003). Regarding SNA, there are some studies suggesting its influence (Paeth and Friederichs 2004; Rodríguez-Fonseca et al. 2006), although there are some authors proposing that SNA SST has a passive role or very limited effects on WA rainfall (Ward 1998; Mo et al. 2001; Vizy and Cook 2001). For this reason, a discussion about the covariability between SNA and the Mediterranean Sea SST anomalies and WA rainfall is considered in this section.

To separate the possible contribution of the Mediterranean Sea SST anomalies from those of the SNA on the summer WA anomalous rainfall, we have performed two different EMCA analyses—one between the Mediterranean Sea and the WA rainfall, and another between the TA and the WA rainfall. The leading EMCA mode, obtained when considering just the Mediterranean SST anomalies (Fig. 9a), explains more than 33% of the covariance and is a very robust mode. The mode relates positive SST over the Mediterranean, maximum at the east, with increasing rainfall over the Sahel, in particular over the 10°–25°N, 5°–25°E region. The correlation of the precipitation expansion coefficient is statistically significant with both, with the first WA rainfall PC in Fig. 2a, and the second EMCA rainfall expansion coefficient in Fig. 3 (0.96 and 0.90, respectively; see Table 1). The same analysis done just for the TA SST presents a second mode (Fig. 9b), with
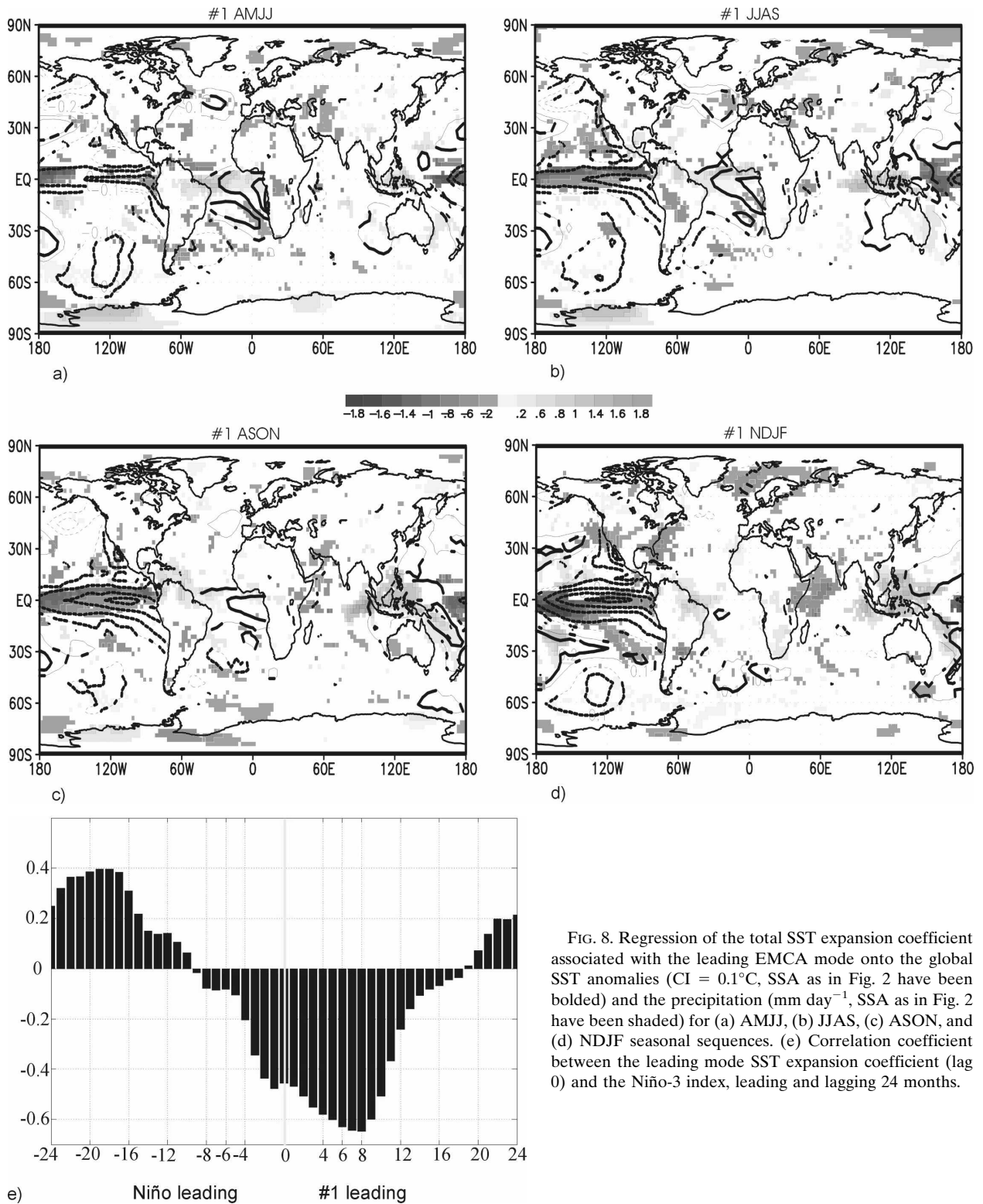
FIG. 8. Regression of the total SST expansion coefficient associated with the leading EMCA mode onto the global SST anomalies (CI = 0.1°C, SSA as in Fig. 2 have been bolded) and the precipitation (mm day$^{-1}$, SSA as in Fig. 2 have been shaded) for (a) AMJJ, (b) JJAS, (c) ASON, and (d) NDJF seasonal sequences. (e) Correlation coefficient between the leading mode SST expansion coefficient (lag 0) and the Niño-3 index, leading and lagging 24 months.
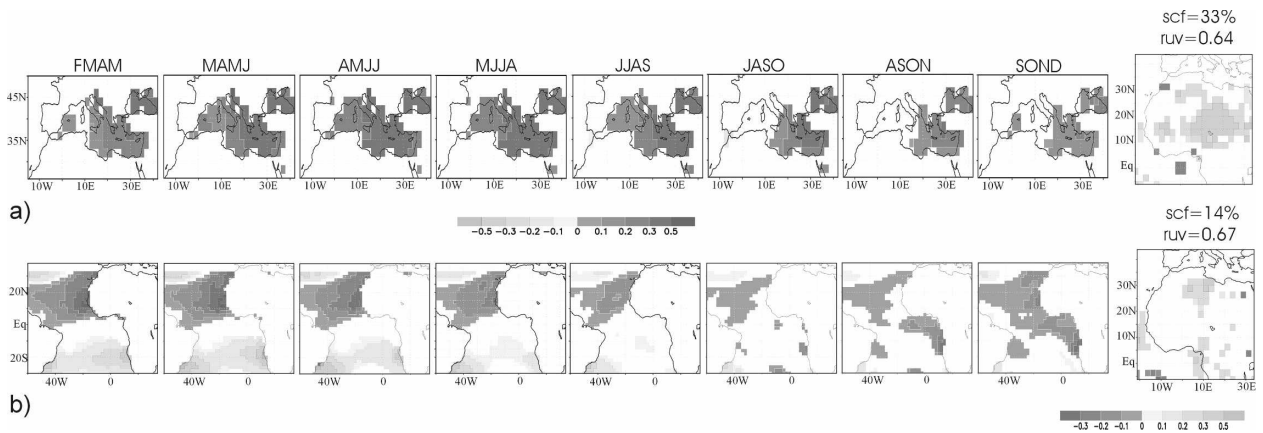
FIG. 9. (a) Leading covariability mode obtained from the EMCA between summer WA precipitation and the anomalous Mediterranean Sea SST 4-month sequences from FMAM to SOND. Only SSA as in Fig. 2 have been shaded. (b) Second covariability mode obtained from the EMCA between summer WA precipitation and the anomalous TA SST (avoiding the Mediterranean Sea) corresponding to the 4-month sequences from FMAM to SOND. Only SSA as in Fig. 2 have been shaded.

maximum loadings over the Congo River basin and the northern Sahel region. This pattern is itself more related to the third mode of variability when including the Mediterranean (not shown; the correlation coefficient between the both SST expansion coefficients is 0.83).

The correlation coefficients between the expansion coefficients of the three analyses are presented in Table 1. The three precipitation EMCA expansion coefficients obtained for the three EMCA analyses (tropical Atlantic + Mediterranean, Mediterranean, and tropical Atlantic) are significantly correlated with the leading WA rainfall PC. However, regarding the SST expansion coefficients, the result from the total analysis (tropical Atlantic + Mediterranean) is very similar to the TA analysis ($r = 0.71$), but is less significant for the Mediterranean Sea analysis ($r = 0.49$), and there is a very poor correlation between TA and the Mediterranean Sea analyses ($r = 0.09$).

These results imply that both the TA and Mediterranean Sea SST anomalies covary with the anomalous

WA precipitation, but not necessary in the same way. Indeed, the sum of the SST expansion coefficients of both analyses, considering the SNA and Mediterranean Sea separately (Fig. 9), is very similar to the SST expansion coefficient of the tropical Atlantic + Mediterranean mode (Fig. 3, lower panel), with a correlation coefficient of 0.82 versus the low correlations in Table 1. This linear relationship evidences that the Mediterranean Sea and the SNA SST are independent components of the WA rainfall variability: the Mediterranean Sea SST influences Sahelian rainfall, while SNA SST influences Congo River basin rainfall.

To characterize the large-scale ocean pattern associated with these two modes, the regression of the SST expansion coefficients onto the global SST anomalies is performed (Figs. 10a,b). The analysis reveals that both large-scale patterns are different. On the one hand, tropical SST anomalies related to the Mediterranean mode are confined to the Pacific. On the other hand, for the SNA mode, the whole tropical ocean basin is

TABLE 1. Correlation coefficients between precipitation expansion coefficients ($U$) and SST expansion coefficients ($V$) from the different EMCA modes (Fig. 3, lower panel and Fig. 9), and WA rainfall PC modes (Fig. 2).

| | Tropical Atlantic (second mode) | Mediterranean Sea (first mode) | First PC WAM | Tropical Atlantic + Mediterranean (third mode) | |
|---|---|---|---|---|---|
| Tropical Atlantic + Mediterranean (second mode) | 0.75 | 0.90 | 0.89 | | $U$ |
| | 0.71 | 0.49 | 0.41 | | $V$ |
| Tropical Atlantic (second mode) | | 0.49 | 0.49 | 0.36 | $U$ |
| | | 0.09 | 0.12 | 0.83 | $V$ |
| Mediterranean Sea (first mode) | | | 0.96 | | $U$ |
| | | | 0.48 | | $V$ |

a)



b)



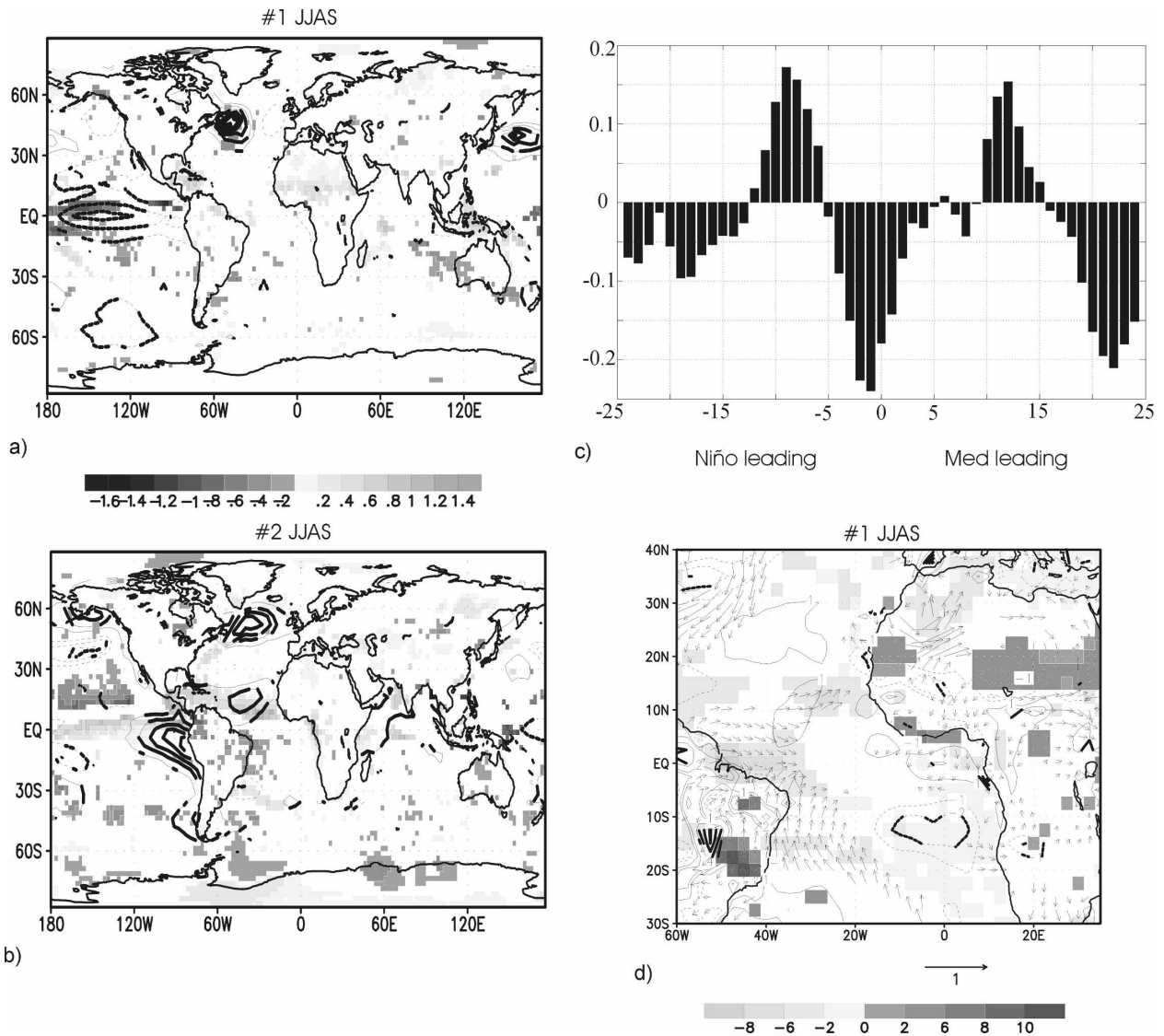c)          Niño leading          Med leading



d)

FIG. 10. (a) Regression of the total SST expansion coefficient associated with the Mediterranean Sea EMCA leading mode onto the global SST anomalies (CI = 0.1°C, SSA as in Fig. 2 have been bolded) and the precipitation (mm day$^{-1}$, SSA as in Fig. 2 have been shaded) for JJAS. Note that SST anomalies over the Mediterranean Sea are significant (same as Fig. 9a), but the contour lines in the global map are not visible enough. (b) Same as (a), but for the total SST expansion coefficient associated with the TA EMCA second mode. (c) Correlation coefficient between the total SST expansion coefficient associated with the Mediterranean Sea EMCA leading mode (lag 0) and the Niño-3 index, leading and lagging 24 months. (d) Regression of the total SST expansion coefficient associated with the Mediterranean Sea EMCA leading mode onto the radiative flux anomalies (shortwave minus longwave radiation, W m$^{-2}$, positive downward, only SSA as in Fig. 2 have been shaded), the surface wind anomalies (vectors, m s$^{-1}$, only SSA as in Fig. 2, have been plotted), and the latent heat flux anomalies (CI = 1 W m$^{-2}$, positive downward, only SSA as in Fig. 2 have been contoured) for the JJAS season.

also significant. The SST signal over the Pacific is also different for both modes: the Mediterranean mode is related to central equatorial Pacific SST, while the SNA mode is related to the central-eastern equatorial Pacific.

The central equatorial Pacific SST signal related to the Mediterranean mode corresponds to the evolution of an extratropical Pacific mode from the previous sum-

mer (not shown), but not to a canonical El Niño event. However, the lead–lag correlation analysis between the Mediterranean expansion coefficient and the Niño-3 index shows, with weak but significant scores, a 2-yr correlation cycle that could give some insight into predictability issues (Fig. 10c). Hence, the previously suggested connection between tropical Pacific SST and Sahelian rainfall (Janicot et al. 1996; Janicot et al. 2001)

seems to be pointing at the Mediterranean Sea as a relevant mediator. Thus, the relationship could be interpreted as a tropical Pacific–Mediterranean–Mediterranean–Sahel interaction. The physical mechanisms involved in the remote relation between Mediterranean and Pacific SST anomalies (Fig. 10a) could include atmospheric teleconnections through Rossby waves. In addition, significant simultaneous correlations are found between Pacific decadal oscillation index and the Mediterranean mode. This is an important area of research in progress by the authors through observational and model analyses. However, it is worthwhile to notice that the regression of the leading WA rainfall PC (from Fig. 2a) onto the global SST anomalies is significant only over the Mediterranean Sea region (not shown), giving robust weight to the Mediterranean influence during the dry Sahel period.

Regarding the large-scale SST signal related to the SNA mode, Fig. 10b yields both a North Atlantic pattern, which is reminiscent of the previous winter tripole SST pattern (not shown), and a tropical Pacific pattern, which resembles the decay phase of El Niño (the remaining eastern anomaly accompanied by the opposite western surrounding one). Some authors have pointed out the manner in which ENSO phenomenon can warm the SNA through the Pacific–North America (PNA) pattern and via Atlantic Walker-related anomalies (Wang 2002b; Kushnir et al. 2006), while the NAO modulates trade wind strength and, in turn, SNA SST (Okumura et al. 2001). The regressed precipitation for this SNA mode shows positive anomalous rainfall over the eastern equatorial Pacific, the Western Hemisphere warm pool (Wang 2002b), and the Congo River basin region, and negative loadings over northeastern Brazil.

Our results conclude that interannual Sahelian rainfall variability for the 1979–2002 period is mainly related to Mediterranean SST anomalies, instead of the Pacific basin or SNA region. Figure 10d shows the Mediterranean SST expansion coefficient regressed onto the surface wind, latent heat flux, and radiation flux anomalies for the JJAS season. There is a positive radiative flux anomaly over the Sahel region, which means that the Mediterranean influence is mainly nonconvective. The monsoon flow is weak, and the Harmattan winds over the Sahel are strengthened. This result coincides with those of Rowell (2003), who has shown that in years in which Mediterranean SSTs are warmer than average, increased evaporation leads to an enhanced moisture content of the air that is advected southward by the low-level mean flow across the eastern Sahara into the Sahel, feeding the increased moisture convergence and leading to increased rainfall. Jung et al. (2006) simulates the 2003 Mediterranean warm

event, showing how the anomalously high moisture is advected from the Mediterranean by the climatological Harmattan and Etesian winds, where enhanced moisture flux convergence leads to more precipitation. Rowell (2003) also shows how the additional heating over the Sahel could induce a stronger low-level inflow from the TA, which can be an explanation for the appearance of the Mediterranean and SNA SST anomalies together associated with anomalous Sahel rainfall.

## 4. Conclusions

This work characterizes the most relevant observational TA (and Mediterranean Sea) SST modes coupled to the summer WA rainfall, in order to understand the possible predictability of the interannual WA rainfall variability for the Sahel dry period. We have evidenced the reliability of the precipitation dataset as well as the use of EMCA technique as a tool for resolving time-evolving SST patterns in relation to the anomalous WA rainfall. Using the CMAP rainfall dataset for the 1979–2002 period, the first two summer WA rainfall EOF variability modes have been determined as Sahelian and Guinean rainfall patterns, which appear as uncoupled ones. In contrast to other works that use the CRU dataset, different time periods, and/ or different methodologies, no evidence for a dipole pattern is found for this period.

The leading SST–precipitation EMCA mode shows the evolution of the equatorial Atlantic mode associated with anomalous precipitation over the coast of the GG. The SST pattern is persisting for almost the complete sequence. Results suggest that the origin of the SST pattern occurs at the Angola/Benguela upwelling area because of an anomalous alongshore wind stress over this region. The wind anomalies over the southeast Atlantic could be associated with a previous anomalous subsidence over the Amazon basin. The eastern anomalous SST creates a zonal gradient over the equatorial band, changing the thermocline slope. The SLA associated with the SST propagates westward as a Rossby oceanic wave from the southeastern Atlantic as far as the west-central equatorial Atlantic. A different sign SLA anomaly, induced by anomalous Ekman pumping at the west Atlantic, propagates eastward as Kelvin oceanic wave, helping to damp the EM. The latent heat flux anomalies and the reversion of the wind anomalies also contribute to restore the normal conditions over the TA. Nevertheless, in order to assess these hypotheses about the EM air–sea interactions, a coupled model would be needed.

We have also evidenced that the leading TA EMCA mode could be important in driving Pacific anomalies.

This different equatorial Pacific–Atlantic connection during the dry Sahel period implies a less active role of the ENSO events on the Sahelian rainfall anomalies, while the Pacific–Atlantic relationship has more influence on the rainfall over the coast of the GG, because the Walker circulation is anomalous along the entire equatorial band.

Although the Atlantic El Niño mode by itself does not seem to have a large influence on Sahelian rainfall, a seasonal correlation between autumn Guinean rainfall and the following summer Sahel rainfall has been found and evaluated by other authors, mainly as the result of the soil moisture conditions persistence and the developed vegetation interactions (Philippon and Fontaine 2002; Fontaine et al. 2002; Douville et al. 2007).

The second SST–WA rainfall covariability mode relates the anomalous Sahelian rainfall to an anomalous SST pattern over the SNA and Mediterranean Sea. This mode shows how, from AMJJ to JJAS, the warm Mediterranean SST anomalies enhance the Sahel precipitation by more evaporation and southward low-level flow to the Sahel. The westerly winds from the Atlantic are also favored, strengthening the deep and dry convection over the Sahara low. Different EMCA analyses have shown that the Mediterranean SST pattern has the major contribution on Sahel rainfall, while the direct influence of the SNA is not clear. The global SST pattern associated with the Mediterranean Sea mode shows SST anomalies over the central Pacific and North Atlantic. It suggests that the Pacific–Sahel connection could be via the Mediterranean Sea. However, during this period, the Sahelian rainfall variability seems to be influenced only by the Mediterranean Sea (the leading WA rainfall PC regressed onto global SST has shown significant SST anomalies just over the Mediterranean Sea).

This work outlines the TA role over the WA rainfall, indicating that for the 1980s and 1990s the EM is the most relevant mode affecting the GG region and there is no significant link with the Sahelian rainfall. The Mediterranean is shown to affect just over the Sahel precipitation. Nevertheless, there are some constraints that should be outlined. On the one hand, the ocean is not the only factor explaining the WA rainfall variability, and the interaction with land surface processes and the role played by soil moisture and vegetation are also crucial factors (Douville 2002; Philippon and Fontaine 2002). On the other hand, the Atlantic Ocean is not the only basin that influences WA rainfall variability. The role of other ocean basins has been also analyzed in an intercomparison exercise that is being developed in the framework of the AMMA-EU project. In this work, the same analysis for different ocean basins has been done, finding that, for this period, the Mediterranean Sea SST anomalies are the most important in driving Sahel anomalies, while the central Pacific SST and eastern Indian Ocean SST explains less than 10% and 14%, respectively, of the SST–WA rainfall covariability, and the SST evolution of those patterns is not very clear.

## REFERENCES

Bader, J., and M. Latif, 2003: The impact of decadal-scale Indian Ocean sea surface temperature anomalies on Sahelian rainfall and the North Atlantic Oscillation. *Geophys. Res. Lett.,* **30,** 2169, doi:10.1029/2003GL018426.

Barreiro, M., A. Giannini, P. Chang, and R. Saravanan, 2004: On the role of the South Atlantic atmospheric circulation in tropical Atlantic variability. *Earth's Climate: The Ocean-Atmosphere Interaction, Geophys. Monogr.,* Vol. 147, Amer. Geophys. Union, 143–156.

Bretherton, S. B., C. Smith, and J. H. Wallace, 1992: An intercomparison of methods for finding coupled patterns in climate data. *J. Climate,* **5,** 541–560.

Carton, J. A., X. Cao, B. S. Giese, and A. M. Da Silva, 1996: Decadal and interannual SST variability in the tropical Atlantic Ocean. *J. Phys. Oceanogr.,* **26,** 1165–1175.

Chang, P., L. Ji, and H. Li, 1997: A decadal climate variation in the tropical Atlantic Ocean from thermodynamic air–sea interactions. *Nature,* **385,** 516–518.

Chelton, D. B., and M. G. Schlax, 1996: Global observations of oceanic Rossby waves. *Science,* **272,** 234–238.

Douville, H., 2002: Influence of soil moisture on the Asian and African monsoons. Part II: Interannual variability. *J. Climate,* **15,** 701–720.

——, S. Conil, S. Tyteca, and A. Voldoire, 2007: Soil moisture memory and West African monsoon predictability: Artefact or reality? *Climate Dyn.,* **28,** 723–742.

Florenchie, P., J. R. E. Lutjeharms, C. J. C. Reason, S. Masson, and M. Rouault, 2003: The source of Benguela Niños in the South Atlantic Ocean. *Geophys. Res. Lett.,* **30,** 1505, doi:10.1029/2003GL017172.

Folland, C. K., T. N. Palmer, and D. E. Parker, 1986: Sahel rainfall and worldwide sea temperatures. *Nature,* **320,** 602–607.

Fontaine, B., and S. Janicot, 1996: Sea surface temperature fields associated with West African rainfall anomaly types. *J. Climate,* **9,** 2935–2940.

——, ——, and V. Moron, 1995: Rainfall anomaly patterns and wind field signals over West Africa in August (1958–1989). *J. Climate,* **8,** 1503–1510.

——, N. Philippon, S. Trzaska, and P. Roucou, 2002: Spring to summer changes in the West African monsoon through NCEP/NCAR reanalyses (1968–1998). *J. Geophys. Res.,* **107,** 4186, doi:10.1029/2001JD000834.

——, P. Roucou, and S. Trzaska, 2003: Atmospheric water cycle and moisture fluxes in the West African monsoon: Mean annual cycles and relationship using NCEP/NCAR reanalysis. *Geophys. Res. Lett.,* **30,** 1117, doi:10.1029/2002GL015834.

França, C., I. Wainer, A. R. De Mesquita, and G. J. Goni, 2003: Planetary equatorial trapped waves in the Atlantic Ocean from TOPEX/Poseidon altimetry. *Interhemispheric Water Exchange in the Atlantic Ocean,* G. J. Goni and P. Malanotte-Rizzoli, Eds., Elsevier Oceanography Series, Vol. 68, Elsevier, 213–232.

Frankignoul, C., and E. Kestenare, 2005: Air–sea interactions in the tropical Atlantic: A view based on lagged rotated maximum covariance analysis. *J. Climate,* **18,** 3874–3890.

García-Serrano, J., T. Losada, B. Rodríguez-Fonseca, and I. Polo, 2008: Tropical Atlantic variability modes (1979–2002). Part II: Time-evolving atmospheric circulation related to SST-forced tropical convection. *J. Climate,* **21,** 6476–6497.

Giannini, A., R. Saravannan, and P. Chang, 2003: Oceanic forcing of Sahel rainfall on interannual to interdecadal time scales. *Science,* **302,** 1027–1030.

Handoh, I. C., and G. R. Bigg, 2000: A self-sustaining climate mode in the tropical Atlantic, 1995–97: Observations and modelling. *Quart. J. Roy. Meteor. Soc.,* **126,** 807–821.

Hastenrath, S., 1984: Interannual variability and annual cycle: Mechanisms of circulation and climate in the tropical Atlantic sector. *Mon. Wea. Rev.,* **112,** 1097–1107.

Hill, K. L., I. S. Robinson, and P. Cipollini, 2000: Propagation characteristics of extratropical planetary waves observed in the ATSR global sea surface temperature record. *J. Geophys. Res.,* **105,** 21 927–21 945.

Janicot, S., 1992: Spatiotemporal variability of West African rainfall. Part I: Regionalization and typings. *J. Climate,* **5,** 489–497.

——, V. Moron, and B. Fontaine, 1996: Sahel droughts and ENSO dynamics. *Geophys. Res. Lett.,* **23,** 515–518.

——, A. Harzallah, B. Fontaine, and V. Moron, 1998: West African monsoon dynamics and eastern equatorial Atlantic and Pacific SST anomalies (1970–1988). *J. Climate,* **11,** 1874–1882.

——, S. Trzaska, and I. Poccard, 2001: Summer Sahel-ENSO teleconnection and decadal time scale SST variations. *Climate Dyn.,* **18,** 303–320.

Jung, T., L. Ferranti, and A. M. Tompkins, 2006: Response to the summer of 2003 Mediterranean SST anomalies over Europe and Africa. *J. Climate,* **19,** 5439–5454.

Jury, M. R., D. B. Enfield, and J.-L. Mélice, 2002: Tropical monsoons around Africa: Stability of El Niño–Southern Oscillation associations and links with continental climate. *J. Geophys. Res.,* **107,** 3151, doi:10.1029/2000JC000507.

Keenlyside, N. S., and M. Latif, 2007: Understanding equatorial Atlantic interannual variability. *J. Climate,* **20,** 131–142.

Kushnir, Y., W. A. Robinson, P. Chang, and A. W. Robertson, 2006: The physical basis for predicting Atlantic sector seasonal-to-interannual climate variability. *J. Climate,* **19,** 5949–5970.

Lamb, P. J., 1978: Large-scale tropical Atlantic surface circulation patterns associated with sub-Saharan weather anomalies. *Tellus,* **30,** 240–251.

Latif, M., and A. Grötzner, 2000: On the equatorial Atlantic oscillation and its response to ENSO. *Climate Dyn.,* **16,** 213–218.

Liebmann, B., and C. A. Smith, 1996: Description of a complete (interpolated) outgoing longwave radiation dataset. *Bull. Amer. Meteor. Soc.,* **77,** 1275–1277.

Lu, J., and T. L. Delworth, 2005: Oceanic forcing of the late 20th century Sahel drought. *Geophys. Res. Lett.,* **32,** L22706, doi:10.1029/2005GL023316.

Melice, J. L., and J. Servain, 2003: The tropical Atlantic meridional SST gradient index and its relationships with the SOI, NAO and Southern Ocean. *Climate Dyn.,* **20,** 447–464.

Mo, K., G. D. Bell, and W. M. Thiaw, 2001: Impact of sea surface temperature Anomalies on the Atlantic tropical storm activity and West African rainfall. *J. Atmos. Sci.,* **58,** 3477–3496.

Moron, V., N. Philippon, and B. Fontaine, 2003: Skill of Sahel rainfall variability in four atmospheric GCMs forced by prescribed SST. *Geophys. Res. Lett.,* **30,** 2221, doi:10.1029/2003GL018006.

Motha, R. P., S. K. Leduc, L. T. Steyaert, C. M. Sakamoto, and N. D. Strommen, 1980: Precipitation patterns in West Africa. *Mon. Wea. Rev.,* **108,** 1567–1578.

North, G. R., T. L. Bell, F. Cahalan, and F. J. Moeng, 1982: Sampling errors in the estimation of empirical orthogonal functions. *Mon. Wea. Rev.,* **110,** 699–706.

Okumura, Y., S. P. Xie, A. Numaguti, and Y. Tanimoto, 2001: Tropical Atlantic air–sea interactions and its influence on the NAO. *Geophys. Res. Lett.,* **28,** 1507–1510.

Paeth, H., and P. Friederichs, 2004: Seasonality and time scales in the relationship between global SST and African rainfall. *Climate Dyn.,* **23,** 815–837.

——, and A. Hense, 2004: SST versus climate change signals in West African rainfall: 20th century variations and future projections. *Climatic Change,* **65,** 179–208.

——, and J. Stuck, 2004: The West African dipole in rainfall and its forcing mechanisms in global and regional climate models. *Mausam,* **55,** 561–582.

Philander, S. G. H., 1990: *El Niño, La Niña, and the Southern Oscillation.* International Geophysics Series, Vol. 46, Academic Press, 293 pp.

Philippon, N., and B. Fontaine, 2002: The relationship between the Sahelian and previous second Guinean rainy seasons: A monsoon regulation by soil wetness? *Ann. Geophys.,* **20,** 575–582.

Polito, P. S., and P. Cornillon, 1997: Long baroclinic Rossby waves detected by TOPEX/POSEIDON. *J. Geophys. Res.,* **102,** 3215–3235.

Polo, I., B. Rodríguez-Fonseca, and J. Sheinbaum, 2005: Northwest Africa upwelling and the Atlantic climate variability. *Geophys. Res. Lett.,* **32,** L23702, doi:10.1029/2005GL023883.

——, A. Lazar, and B. Rodríguez-Fonseca, 2008: Oceanic Kelvin waves and tropical Atlantic intraseasonal variability. Part II: Mechanisms and impacts. *J. Geophys. Res.,* **113,** C07009, doi:10.1029/2007JC004495.

Rodríguez-Fonseca, B., I. Polo, E. Serrano, and M. Castro, 2006: Evaluation of the north Atlantic SST forcing on the European and northern African winter climate. *Int. J. Climatol.,* **26,** 179–191, doi:10.1002/joc.1234.

Rowell, D. P., 2001: Teleconnections between the tropical Pacific and the Sahel. *Quart. J. Roy. Meteor. Soc.,* **127,** 1683–1706.

——, 2003: The impact of the Mediterranean SSTs on the Sahelian rainfall season. *J. Climate,* **16,** 849–862.

Servain, J., A. J. Busalacchi, M. J. McPhaden, A. D. Moura, G. Reverdin, M. Vianna, and S. E. Zebiak, 1998: A Pilot Research Moored Array in the Tropical Atlantic (PIRATA). *Bull. Amer. Meteror. Soc.,* **79,** 2019–2032.

Shinoda, M., and R. Kawamura, 1994: Tropical rainbelt, circulation, and sea surface temperatures associated with the Sahelian rainfall trend. *J. Meteor. Soc. Japan,* **72,** 341–357.

Smith, T. M., and R. W. Reynolds, 2003: Extended reconstruction of global sea surface temperatures based on COADS data (1854–1997). *J. Climate,* **16,** 1495–1510.

Sterl, A., and W. Hazeleger, 2003: Coupled variability and air-sea interaction in the South Atlantic Ocean. *Climate Dyn.,* **21,** 559–571, doi:10.1007/s00382-003-0348-y.

Sultan, B., K. Labadi, J. F. Guegan, and S. Janicot, 2005: Climate drives the meningitis epidemics onset in West Africa. *PLoS Med.,* **2,** 43–49.

Tippett, M. K., 2006: Filtering of GCM simulated Sahel precipitation. *Geophys. Res. Lett.,* **33,** L01804, doi:10.1029/2005GL024923.

——, and A. Giannini, 2006: Potentially predictable components of African summer rainfall in a SST-forced GCM simulation. *J. Climate,* **19,** 3133–3144.

Trzaska, S., A. W. Robertson, J. Farrara, and C. R. Mechoso, 2007: South Atlantic variability arising from air-sea coupling: Local mechanisms and tropical–subtropical interactions. *J. Climate,* **20,** 3345–3365.

Uppala, S. M., and Coauthors, 2005: The ERA-40 re-analysis. *Quart. J. Roy. Meteor. Soc.,* **131,** 2961–3012.

Vauclair, F., and Y. du Penhoat, 2001: Interannual variability of the upper layer of the tropical Atlantic Ocean from in situ data between 1979 and 1999. *Climate Dyn.,* **17,** 527–546.

——, ——, and G. Reverdin, 2004: Heat and mass budgets of the warm upper layer of the tropical Atlantic Ocean in 1979–99. *J. Phys. Oceanogr.,* **34,** 903–919.

Venegas, S. A., L. A. Mysak, and D. N. Straub, 1997: Atmosphere–ocean coupled variability in the South Atlantic. *J. Climate,* **10,** 2904–2920.

Vizy, E. K., and K. H. Cook, 2001: Mechanisms by which Gulf of Guinea and eastern North Atlantic sea surface temperature anomalies can influence African rainfall. *J. Climate,* **14,** 795–821.

Wagner, R. G., and A. M. da Silva, 1994: Surface conditions associated with anomalous rainfall in the Guinea coastal region. *Int. J. Climatol.,* **14,** 179–199.

Wang, C., 2002a: Atmospheric circulation cells associated with the El Niño–Southern Oscillation. *J. Climate,* **15,** 399–419.

——, 2002b: Atlantic climate variability and its associated atmospheric circulation cells. *J. Climate,* **15,** 1516–1536.

——, 2006: An overlooked feature of tropical climate: Inter-Pacific-Atlantic variability. *Geophys. Res. Lett.,* **33,** L12702, doi:10.1029/2006GL026324.

Ward, M. N., 1998: Diagnosis and short-lead time prediction of summer rainfall in tropical North Africa at interannual and multidecadal timescales. *J. Climate,* **11,** 3167–3191.

Xie, P., and P. A. Arkin, 1997: Global precipitation: A 17-year monthly analysis based on gauge observations, satellite estimates, and numerical model outputs. *Bull. Amer. Meteor. Soc.,* **78,** 2539–2558.

Zebiak, S. E., 1993: Air–sea interaction in the equatorial Atlantic region. *J. Climate,* **6,** 1567–1586.

Zhang, R., and T. L. Delworth, 2006: The impact of Atlantic multidecadal oscillations on Indian/Sahel rainfall and Atlantic hurricanes. *Geophys. Res. Lett.,* **33,** L17712, doi:10.1029/2006GL026267.